Computer Methods and Programs in Biomedicine 255 (2024) 108369

Contents lists available at ScienceDirect

Computer Methods and Programs in Biomedicine

journal homepage: www.sciencedirect.com/journal/computer-methods-and-programs-in-biomedicine

Pathophysiology of the ascending aorta: Impact of dilation and valve phenotype on large-scale blood flow coherence detected by 4D flow MRI

Karol Calò [a], Andrea Guala [b,c], Valentina Mazzi [a], Maurizio Lodi Rizzini [a], Lydia Dux-Santoy [b], Jose Rodriguez-Palomares [b,c,d], Stefania Scarsoglio [a], Luca Ridolfi [e], Diego Gallo [a,*], Umberto Morbiducci [a]

[a] PolitoBIOMed Lab, Department of Mechanical and Aerospace Engineering, Politecnico di Torino, Turin, Italy
[b] Vall d'Hebron Institut de Recerca, Barcelona, Spain
[c] Biomedical Research Networking Center on Cardiovascular Diseases, Instituto de Salud Carlos III, Madrid, Spain
[d] Department of Cardiology, Hospital Universitari Vall d'Hebron, Barcelona, Spain
[e] PolitoBIOMed Lab, Department of Environment, Land and Infrastructure Engineering, Politecnico di Torino, Turin, Italy

ARTICLE INFO

Keywords:
4D flow MRI
Aortic dilation
Bicuspid aortic valve
Flow coherence
Hemodynamics
Spatiotemporal analysis

ABSTRACT

Background and objective: The evidence on the role of hemodynamics in aorta pathophysiology has yet to be robustly translated into clinical applications, to improve risk stratification of aortic diseases. Motivated by the need to enrich the current understanding of the pathophysiology of the ascending aorta (AAo), this study evaluates *in vivo* how large-scale aortic flow coherence is affected by AAo dilation and aortic valve phenotype.
Methods: A complex networks-based approach is applied to 4D flow MRI data to quantify subject-specific AAo flow coherence in terms of correlation between axial velocity waveforms and the aortic flow rate waveform along the cardiac cycle. The anatomical length of persistence of such correlation is quantified using the recently proposed network metric average weighted curvilinear distance (*AWCD*). The analysis considers 107 subjects selected to allow an ample stratification in terms of aortic valve morphology, absence/presence of AAo dilation and of aortic valve stenosis.
Results: The analysis highlights that the presence of AAo dilation as well as of bicuspid aortic valve phenotype breaks the physiological AAo flow coherence, quantified in terms of *AWCD*. Of notice, it emerges that cycle-average blood flow rate and relative AAo dilation are main determinants of *AWCD*, playing opposite roles in promoting and hampering the persistence of large-scale flow coherence in AAo, respectively.
Conclusions: The findings of this study can contribute to broaden the current mechanistic link between large-scale blood flow coherence and aortic pathophysiology, with the prospect of enriching the existing tools for the *in vivo* non-invasive hemodynamic risk assessment for aortic diseases onset and progression.

1. Introduction

The aneurysm of the ascending thoracic aorta constitutes a common cardiovascular disease that entails a high risk of life-threatening complications such as aortic dissection or rupture. Thoracic aortic aneurysm (TAA) often develops silently until adverse events occur, with the consequence that short- and long-term survival outcomes deteriorate rapidly [1]. In this regard, TAAs are a common cause of premature deaths with an estimated mortality of 150,000–200,000 deaths per year worldwide [2]. With respect to clinical management, no medical therapy has been proven effective in reducing the growth or rupture of TAAs. Usually, the maximum aortic diameter has been considered the main predictor of complications and, therefore, relevant Clinical Practice Guidelines adopt this parameter to recommend preventive surgical substitution of the aneurysm [3]. However, the aortic size criterion for surgical intervention is widely recognized to be a poor prognostic biomarker for aneurysms complications [4].

One recognized risk factor linked to ascending aorta (AAo) dilation is bicuspid aortic valve (BAV) [5–7], a congenital heart defect affecting approximately 1–2 % of the general population [5]. The 60–70 % of all ascending aneurysms in BAV patients involve the tubular AAo, namely the portion between the sinotubular junction (STJ) and the aortic arch

* Corresponding author.
E-mail address: diego.gallo@polito.it (D. Gallo).

https://doi.org/10.1016/j.cmpb.2024.108369
Received 16 May 2024; Received in revised form 22 July 2024; Accepted 7 August 2024
Available online 8 August 2024

[8]. The etiology of BAV aortopathy, and in general of TAAs, is still debated. Some evidence supports the hypothesis that the weakening of the aortic wall is mainly a result of genetic alterations [9,10], but it is clear that genetics is unlikely to be the sole causal mechanism for AAo dilation in BAV [7,11].

In this context, there is a broad consensus regarding the involvement of hemodynamics in the onset and progression of aortic disease, especially in BAV patients. Among the most relevant observations, patients with dilated AAo commonly present with deranged blood flow patterns [12–14] such as eccentric outflow jet in the proximal AAo, and markedly unphysiological helical and/or vortical flow [15], which have been positively associated with AAo diameter [14] and with the presence of abnormal valve phenotypes [16–18]. In this framework, also aortic stenosis (AS) plays an important role in altering the hemodynamic structures downstream of the aortic valve [15,19], which later break up into smaller turbulent eddies [20–22]. Aortic hemodynamic abnormalities also reflect in near-wall flow disturbances, which are significantly correlated with wall structural degradation [13,23–25]. Corroborating this concept, several studies [6,26–30] have reported of abnormal transvalvular flows with increased peak velocity, increased energy losses and a highly eccentric flow jet impinging on the outer aortic wall in BAV patients. However, the link between the aortic pathophysiology and the way the large-scale fluid structures are advected through the aorta (eventually conditioned by the coexistence of AAo dilation and valve abnormalities) has not yet been fully elucidated, with most of the studies providing a characterization of the aortic hemodynamics limited to instantaneous snapshots or time- and space-averaged flow quantities. This reductionist approach, dictated by the need to provide clinically oriented diagnostic and prognostic tools synthesizing the four-dimensional hemodynamic complexity, inherently overlooks relevant features enclosed in blood flow dynamics, which can be altered in presence of aortic diseases.

In the attempt to explore the consequence of this information loss, a characterization of large-scale coherent motion has been recently proposed interpreting arterial flows as “social networks” and applying the Complex Networks (CNs) Theory [31,32]. *In silico* and *in vivo* studies adopting a CNs-based approach have suggested that AAo dilation breaks the physiological spatiotemporal similarity of the large-scale fluid structures in aorta [33], which might be further compromised in the presence of a concomitant BAV [24]. An approach based on the so-called *“one-to-all”* networks, built up to assess local aortic flow similarity to the proximal AAo flow rate waveform [34,35] (considered as main driving factor in shaping large-scale dominant AAo blood flow patterns [26,36,37]) was recently applied to 4D flow MRI data of healthy subjects with normal functioning tricuspid aortic valves (TAVs) to provide reference values for the physiological anatomical length of persistence of coherent AAo flow structures [34].

Building upon the findings from healthy aortas, this study aims to identify the factors involved in the disruption of the physiological coherence of large-scale blood flow patterns in the AAo in the presence of AAo dilation and BAV. The overarching hypothesis of this study is that (i) aortic disorders cause a reduction of the anatomical length of persistence of hemodynamic coherence in the large-scale fluid motion that can be effectively quantified using the network approach, and that (ii) specific features of proximal AAo flow and aortic anatomy markedly contribute to either preserving or disrupting blood flow coherence. Moreover, it is also hypothesized that concomitant aortopathy and valve abnormality can act differently or synergistically to determine the anatomic length of persistence of the coherence in aortic large-scale fluid structures as they are advected through the AAo.

2. Materials and methods

2.1. Study population

A total of 107 adult subjects (>18 years of age) with native aortic valves and free from connective tissue disorders and from previous aortic intervention, dissection and coarctation, and with no contraindication for MRI were enrolled in this study. Participants were selected to allow for an ample stratification for aortic valve morphology (TAV, BAV), absence/presence of AAo dilation (NoDIL, DIL) and of aortic valve stenosis (NoAS, AS), respectively (Table 1).

In detail, 66 patients were diagnosed with at least one of the following conditions: BAV ($n = 43$), dilated DIL AAo ($n = 40$), and mild-to-severe AS ($n = 20$). Healthy subjects ($n = 41$) presenting with normally functioning TAV were also enrolled. Demographic and clinical data of the population under study are reported in Table 1. The cohorts accounting for aortic valve morphology, AAo dilation and aortic valve stenosis did not differ in terms of sex and body surface area (BSA). TAV and BAV patients did not differ also in terms of blood pressure and age, and NoAS and AS patients in terms of blood pressure (Table 1).

AAo maximum diameter and aortic root maximum diameter were measured from cine MRI, and AAo dilation was adjudicated via the calculation of z-score accounting for sex, age and BSA according to reference values [38].

Aortic valve morphology was adjudicated using a stack of balanced steady-state free-precession cine images of the aortic valve. Following American cardiology and surgical guidelines [39], subjects with maximum transvalvular flow velocity measured by echocardiography $V_{max}^{echo} \geq 2$ m s^{-1} were adjudicated presenting with AS.

The recruitment and research procedures were performed in accordance with the principles of the Declaration of Helsinki. The study was approved by the local ethical review board of the Vall d’Hebron University Hospital (approval n° PR(AG)363/2016) and all participants gave written informed consent.

2.2. 4D flow MRI acquisition protocol and data processing

Cardiac MRI data were acquired without intravenous contrast injection on a GE 1.5-T Signa scanner (GE Healthcare, Waukesha, Wisconsin). The protocol included several balanced steady-state free-precession cine images and a 4-dimensional (4D) phase-contrast cardiac MRI (4D flow CMR) acquisition [40] with retrospective ECG gating during free breathing covering the whole thoracic aorta. Data were acquired using the following parameters: field of view 400×400×400 mm, voxel size 2.5×2.5×2.5 mm, flip angle 8°, repetition time 4.2 to 6.4 ms, echo time 1.9 to 3.7 ms, and a reconstructed temporal resolution of 22.3 to 51.5 ms. Maximum velocity encoding was set after measuring maximum blood velocity at the aortic valve from 2D phase-contrast imaging and ranged between 200 and 520 cm s^{-1}. Data were corrected for background phase from concomitant gradients, eddy currents, and trajectory errors of the 3-dimensional radial acquired k-space [40]. Brachial systolic and diastolic pressures were taken immediately after the CMR study.

Each thoracic aorta was semi-automatically segmented from an angiogram derived from 4D-flow. To ensure that a region of interest was consistently identified in all the aortas under investigation [33,34], the AAo was defined as the aortic portion extending from the STJ to the brachiocephalic artery bifurcation, using anatomic landmarks identified from co-registered 2D cine images (Fig. 1).

2.3. Large-scale flow coherence in ascending aorta

A network-based approach was adopted to investigate and quantify the coherence of large-scale AAo fluid structures in terms of similarity to the subject-specific inlet blood flow rate waveform, here considered as driving waveform of the aortic flow as extensively reported in previous studies [31,34,35]. Briefly, the network-based analysis was focused on the axial (through-plane) blood velocity component V_{ax} waveforms along the cardiac cycle, calculated by projecting the local velocity vector measured in each voxel at each acquired phase along the direction

Table 1
Demographic and clinical data of the population under study stratified in cohorts accounting for: aortic valve morphology (TAV, BAV), absence/presence of AAo dilation (NoDIL, DIL) and of aortic valve stenosis (NoAS, AS). Data are presented as median value (interquartile range, IQR) or frequency counts (percentage). Differences between two groups of patients were assessed using Mann-Whitney U tests. Statistical significance is indicated with: $*p < 0.05$; $\dagger p < 0.01$; $\ddagger p < 0.001$; –: non-significant. BSA: body surface area; D_{max}: AAo maximum diameter; D_{root}: aortic root maximum diameter; SBP: systolic blood pressure; DBP: diastolic blood pressure.

	TAV		BAV		p	NoDIL		DIL		p	NoAS		AS		p
N°	64		43			67		40			87		20		
	NoDIL (AS)	DIL (AS)	NoDIL (AS)	DIL (AS)		TAV (AS)	BAV (AS)	TAV (AS)	BAV (AS)		TAV (DIL)	BAV (DIL)	TAV (DIL)	BAV (DIL)	
N°	44 (3)	20 (5)	23 (4)	20 (8)		44 (3)	23 (4)	20 (5)	20 (8)		56 (15)	31 (12)	8 (5)	12 (8)	
Age [years]	46.5 (32.7-70.2)		55.0 (42.7-65.5)		–	42.9 (30.5-49.5)		66.9 (56-72.2)		‡	47 (34.7-62.5)		66.9 (55.5-75)		‡
Men [N, (%)]	43 (67)		29 (67)		–	43 (64)		29 (72)		–	60 (69)		12 (60)		–
BSA [m2]	1.84 (1.67-1.96)		1.83 (1.68-1.95)		–	1.81 (1.64-1.93)		1.91 (1.73-2.03)		–	1.83 (1.69-1.96)		1.82 (1.62-1.95)		–
Dmax [mm]	33.2 (28.9-45.1)		41.4 (36.0-50.8)		†	32.4 (28.5-36.8)		53.6 (47.6-55.6)		‡	35.0 (30.6-45.3)		47.9 (40.8-55.4)		‡
Droot [mm]	32.5 (27.7-37.2)		36.0 (32.0-39.0)		*	32.0 (28.0-34.5)		39.0 (36.0-43.0)		‡	33.0 (29.0-38.5)		34.0 (30.7-38.2)		–
SBP [mmHg]	125.0 (115.7-139.2)		132.0 (121.5-144.5)		–	123.0 (115-135)		135.5 (126-145.5)		†	126.0 (116-136.5)		139.5 (127.7-156.5)		–
DBP [mmHg]	70.5 (60.7-81.5)		75.0 (70.0-84.5)		–	70.0 (63.0-78.0)		79.0 (71.0-88.0)		‡	74.0 (64.0-81.0)		77.5 (69.25-98.0)		–

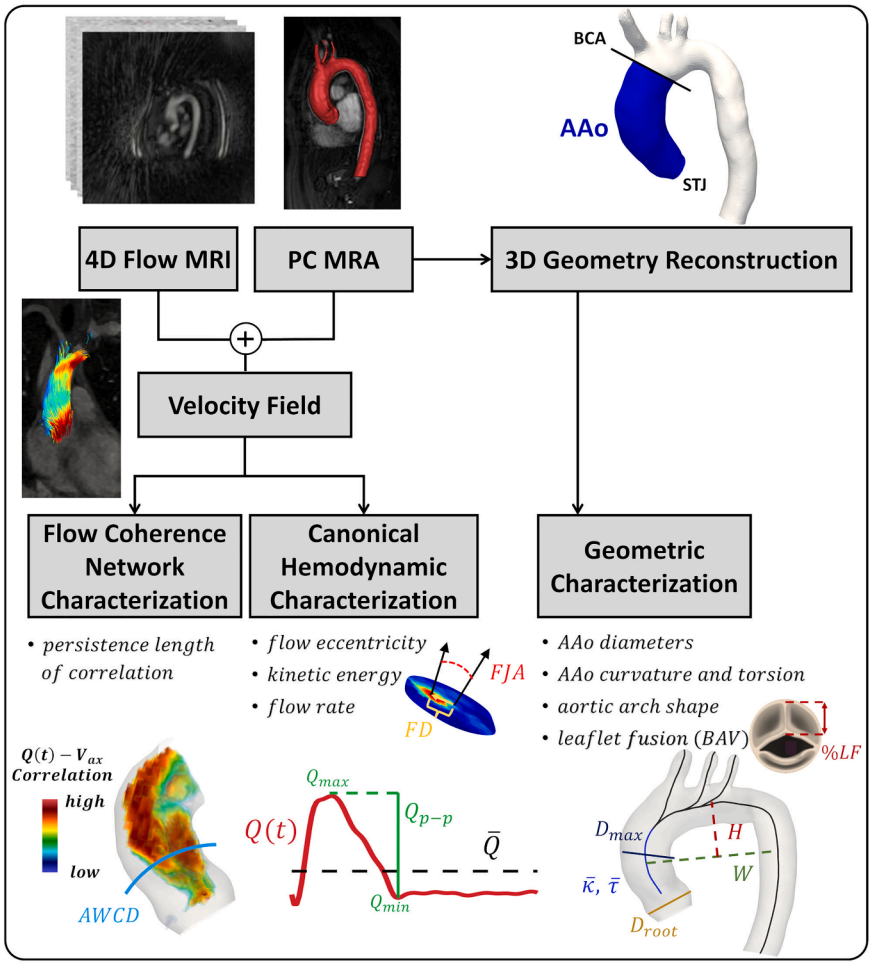

Fig. 1. Schematic diagram of the study design, highlighting how 4D flow MRI data contribute to perform the *in vivo "one-to-all"* network analysis as well as the canonical hemodynamic and geometric characterizations in AAo. PC MRA: phase-contrast MR angiography; STJ: sinotubular junction; BCA: brachiocephalic artery; AAo: ascending aorta; *AWCD*: average weighted curvilinear distance; *FJA*: flow jet angle; *FD*: flow displacement; Q_{max}: maximum value of blood flow rate $Q(t)$; Q_{min}: minimum value of $Q(t)$; $\overline{Q}$: cycle-average aortic blood flow rate; Q_{p-p}: flow rate peak-to-peak amplitude; D_{max}: AAo maximum diameter; D_{root}: aortic root maximum diameter; $\bar{\kappa}$: AAo average curvature; $\bar{\tau}$: AAo average torsion; *H*: aortic arch height; *W*: aortic arch width; %*LF*: percentage of aortic leaflet fusion.

identified by the tangent to the local vessel centerline [31,41]. The axial velocity V_{ax} accounts for the net transport of blood from the heart to organs, being aligned with the main flow direction (with positive (negative) values of V_{ax} indicating anterograde (retrograde) flow [33], Fig. 2). For each subject, V_{ax} waveforms in the AAo fluid domain were used to build a *"one-to-all"* network (Fig. 2) consisting of: (1) one reference node represented by the blood flow rate waveform $Q(t)$, computed from the phase-contrast velocity data, located at the STJ

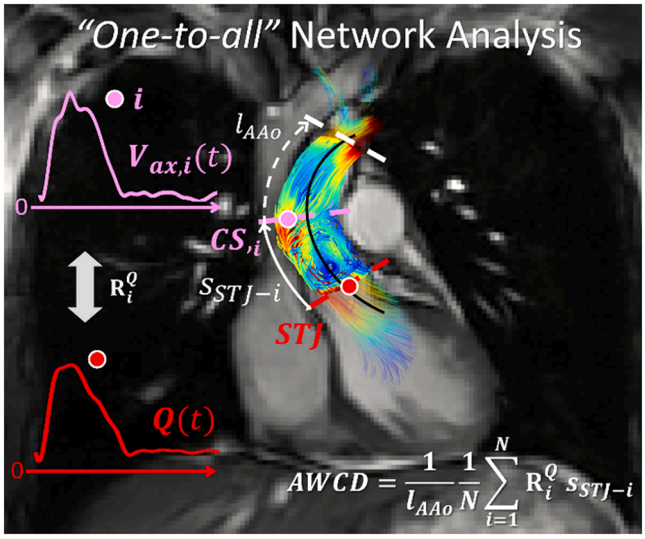

Fig. 2. Methodology for the *in vivo "one-to-all"* network analysis. STJ: sino-tubular junction; *CS,i*: cross-section containing node *i*; s_{STJ-i}: curvilinear distance between node *i* and the reference node at STJ; l_{AAo}: curvilinear length of the AAo centerline; *N*: number of voxels (nodes) in the AAo; R_i^Q: Pearson correlation coefficient between $Q(t)$ and $V_{ax,i}(t)$ waveforms.

section's center of mass; (2) the *N* nodes represented by the axial velocity waveforms $V_{ax,i}(t)$ at all voxels belonging to the AAo region of interest distal to the STJ. The link between the reference node and the generic *i-th* node was weighted using the Pearson correlation coefficient R_i^Q between $Q(t)$ and $V_{ax,i}(t)$ waveforms along the cardiac cycle, thus measuring the dynamic similarity of the voxel-based axial velocity waveform with the driving aortic flow rate. Finally, the anatomical length of persistence of the $Q(t)$ - $V_{ax}(t)$ correlation was quantified using the network-based metric *Average Weighted Curvilinear Distance* (*AWCD*) defined as [34,35]:

$$AWCD = \frac{1}{l_{AAo}} \frac{1}{N} \sum_{i=1}^{N} R_i^Q \, s_{STJ-i}, \tag{1}$$

where l_{AAo} is the curvilinear length of the AAo centerline, *N* is the number of voxels (nodes) in the AAo region of interest, and s_{STJ-i} is the curvilinear distance between the STJ section and the cross-section containing node *i*, where waveforms $Q(t)$ and $V_{ax,i}(t)$ are defined, respectively (Fig. 2). According to the definition in Eq. (1), *AWCD* measures (within the AAo fluid domain) the average distance, normalized by l_{AAo}, over which the local axial velocity waveforms exhibit similarity with the driving flow rate waveform $Q(t)$, before coherence is lost.

To assess the main factors determining the persistence length of the $Q(t)$ - $V_{ax}(t)$ correlation, statistical associations of *AWCD* with hemodynamic and geometric aortic descriptors were investigated.

2.4. Canonical characterization of the aortic hemodynamics

The main features of the AAo hemodynamics quantifiable from 4D flow MRI data were evaluated, namely the aortic blood flow rate $Q(t)$ average value and dynamics, the eccentricity of the aortic valve systolic outflow jet, and the blood flow kinetic energy (Fig. 1). Specifically, from the flow rate waveform $Q(t)$, the cycle-average aortic blood flow rate $\overline{Q}$, the flow rate peak-to-peak amplitude Q_{p-p}, and the pulsatility index Q_{PI} were computed according to [34]:

$$\overline{Q} = \frac{1}{T} \int_0^T Q(t) \, dt, \tag{2}$$

$$Q_{p-p} = Q_{max} - Q_{min}, \tag{3}$$

$$Q_{PI} = \frac{Q_{p-p}}{\overline{Q}}, \tag{4}$$

where *T* is the time duration of the cardiac cycle, and Q_{max} and Q_{min} are the maximum and the minimum values of $Q(t)$, respectively (as reported in Fig. 1).

The AAo systolic flow eccentricity was evaluated in terms of flow jet angle *FJA*, and of normalized flow displacement [42] *FD* (Fig. 1). Briefly, *FJA* measures the angle between the normal vector identifying the aortic cross-section located just distal to the STJ and the direction of the resultant of peak systolic forward flow velocities over the same aortic cross-section. *FD* measures, over the same aortic cross-section as *FJA*, the Eulerian distance between the point of application of the resultant of the peak systolic forward flow velocities - calculated as the average position of lumen voxels, weighted by the velocity magnitude - and the aortic centerline. Both *FJA* and *FD* provide an indication of the severity of flow eccentricity, *e.g.* a consequence of an asymmetric opening of the aortic valve. Moreover, the maximum systolic peak velocity just distal to the STJ was computed for all subjects from 4D flow MRI data and indicated as V_{max}.

The blood kinetic energy (*KE*) associated with large-scale AAo flow was quantified in terms of:

$$\overline{KE}_{avg} = \frac{1}{V_{AAo}} \int_{V_{AAo}} \left[\frac{1}{T} \int_0^T \frac{1}{2} \rho |\mathbf{V}(t)|^2 \, dt \right] dV, \tag{5}$$

$$\overline{KE}_{peak} = \frac{1}{V_{AAo}} \int_{V_{AAo}} \frac{1}{2} \rho \, |\mathbf{V}|^2_{peak} \, dV, \tag{6}$$

where V_{AAo} is the AAo volume, ρ is the blood density (assumed equal to 1060 kg/m^3), and $|\mathbf{V}|_{peak}$ is the magnitude of the blood velocity vector $\mathbf{V}(t)$ at peak systole. Technically, $\overline{KE}_{avg}$ is the *KE* value averaged over the AAo fluid domain and along the cardiac cycle.

2.5. Aortic geometric characterization

The geometric characterization of the AAo anatomy was performed in terms of AAo size, curvature, torsion, and aortic arch shape (Fig. 1), given the suggested role of these anatomical features in shaping the large-scale aortic flow [33,43–47]. In detail, aortic size was characterized from cine MRI in terms of AAo maximum diameter D_{max}, the primary clinical standard for aortic dilation diagnosis [3,48], aortic root maximum diameter D_{root}, and their ratio $D_{ratio} = D_{max}/D_{root}$, a measure of relative AAo dilation [33] (Fig. 1). A centerline-based approach was adopted to evaluate the aortic curvature and torsion, defined as [49]:

$$\kappa(s) = \frac{|\mathbf{C}'(s) \times \mathbf{C}''(s)|}{|\mathbf{C}'(s)|^3}, \tag{7}$$

$$\tau(s) = \frac{[\mathbf{C}'(s) \times \mathbf{C}''(s)] \cdot \mathbf{C}'''(s)}{|\mathbf{C}'(s) \times \mathbf{C}''(s)|^2}, \tag{8}$$

where $\mathbf{C}'(s)$, $\mathbf{C}''(s)$, $\mathbf{C}'''(s)$ are the 1st, 2nd, and 3rd derivatives of the AAo centerline $\mathbf{C}(s)$ over the curvilinear abscissa, respectively. In this study, the average values of curvature ($\bar{\kappa}$) and torsion ($\bar{\tau}$) along the AAo were considered (Fig. 1). A centerline-based approach was also adopted to characterize the shape of the aortic arch in terms of arch width *W* (the Euclidean distance between the centerline points of the AAo and descending aorta at the level of the right pulmonary artery), height *H* (the maximal vertical distance between *W* and the centerline's highest point in the aortic arch), and *H/W* ratio [34] (Fig. 1).

Furthermore, the percentage of aortic leaflet fusion (%*LF*) in BAV patients was investigated (Fig. 1), given the association of leaflet fusion

length with AAo dilation and flow abnormalities in BAVs [50]. Briefly, %*LF* is defined as the ratio between the leaflet fusion length (*i.e.*, the distance, measured in systole, between the commissure and the point where the leaflets separate) and the leaflet length (*i.e.*, the distance, measured in diastole, between the commissure and the point of contact of the leaflets).

2.6. Statistical analysis

Continuous variables were expressed as median value (interquartile range, IQR). Differences between groups of variables were assessed by Mann-Whitney U test, and statistical associations between *AWCD* and the other hemodynamic and geometric quantities were explored using Spearman correlation coefficient (r). In all the performed analyses, statistical significance was assumed for $p < 0.05$. All analyses were performed using MATLAB (The MathWorks, Inc., USA).

3. Results

Firstly, the coherence of the large-scale fluid structures in AAo was analyzed in the entire population. As a second step of the analysis, subjects were stratified into four cohorts and compared according to (i) valve phenotype (TAV *vs.* BAV cohorts), and (ii) presence of aortic dilation (NoDIL *vs.* DIL cohorts). In this regard, a direct comparison NoAS *vs.* AS subjects was not carried out because of the markedly unbalanced size of the two cohorts (Table 1). Finally, the TAV *vs.* BAV and the NoDIL *vs.* DIL comparisons were further broken down along subanalyses by excluding other concomitant pathologies (namely AS, BAV and DIL) from the main cohorts, to isolate their effects on AAo flow coherence. To do that, both TAV and BAV cohorts were further stratified into three subgroups, referred to as (-)AS,DIL (41 subjects in $TAV_{(-)AS,DIL}$ and 19 in $BAV_{(-)AS,DIL}$), (-)AS (56 subjects in $TAV_{(-)AS}$ and 31 in $BAV_{(-)AS}$) and (-)DIL (44 subjects in $TAV_{(-)DIL}$ and 23 in $BAV_{(-)DIL}$) — where (-) indicates the exclusion of the pathology/ies from the cohort — and both NoDIL and DIL groups were stratified into (-)AS,BAV (41 subjects in $NoDIL_{(-)AS,BAV}$ and 15 in $DIL_{(-)AS,BAV}$), (-)AS (60 subjects in $NoDIL_{(-)AS}$ and 27 in $DIL_{(-)AS}$) and (-)BAV (44 subjects in $NoDIL_{(-)BAV}$ and 20 in $DIL_{(-)BAV}$) subgroups.

Analyzing the coherence of the large-scale fluid structures in AAo over the entire population under study, the similarity between $Q(t)$ and $V_{ax}(t)$ waveforms along the cardiac cycle is characterized by a median value $\widehat{R}_i^Q = 0.53$ (0.19–0.75), and a median *AWCD* value equal to 0.24 (0.18–0.32). The volumetric maps of R_i^Q values and the *AWCD* values in AAo are presented in Fig. 3 for four explanatory cases, namely one healthy subject (the one presenting with the maximum *AWCD*) and three patients presenting with the minimum *AWCD* value among only BAV, only DIL, and only AS patients, respectively. In the healthy aorta, strong correlations between the inlet flow rate $Q(t)$ and $V_{ax}(t)$ waveforms are uniformly distributed along the entire AAo fluid domain, and the anatomical length of persistence of the large-scale fluid structures with $Q(t)$ extends to cover 43 % of the AAo curvilinear length (Fig. 3a). On the contrary, in the presence of BAV or AS: (i) connected regions with highest similarity of $Q(t)$ and $V_{ax}(t)$ waveforms (as depicted by the visualized $R_i^Q > \widehat{R}_i^Q$ values) are mainly confined between the AAo axis and the outer wall; (ii) the length of persistence of the correlation between $V_{ax}(t)$ waveforms and the inlet flow rate $Q(t)$ measured by*AWCD* presents values down to 15–16 % of the AAo curvilinear length (Fig. 3b and 3d, respectively). As for the dilated AAo, the length of persistence of the correlation between $V_{ax}(t)$ waveforms and the inlet flow rate $Q(t)$ can be markedly shortened, and the axial flow coherence can persist no more than the 11 % of the total AAo curvilinear length, just distal to the STJ landmark (Fig. 3c).

3.1. Impact of aortic valve phenotype and AAo dilation on large-scale flow coherence

The impact of aortic valve phenotype and AAo dilation on the persistence length of the correlation between $V_{ax}(t)$ waveforms and the inlet flow rate $Q(t)$ was investigated comparing *AWCD* distributions in the TAV *vs.* BAV and NoDIL *vs.* DIL groups, and in the respective subgroups accounting for the effects of concomitant pathologies, as clarified before.

Regarding the impact of the valve phenotype on the large-scale motion coherence in AAo, from the TAV *vs.* BAV comparison (Fig. 4, upper panel) it emerged that *AWCD* is significantly larger in TAV subjects regardless of concomitant pathologies (median value 0.25 (0.20–0.35) *vs.* 0.20 (0.15–0.28) in BAV, $p < 0.01$), or when TAV and BAV subjects are affected by AAo dilation but not AS (*AWCD* 0.30 (0.22–0.35) in $TAV_{(-)AS}$ subgroup *vs.* 0.24 (0.18–0.29) in $BAV_{(-)AS}$, $p < 0.05$). No significant differences emerged, in terms of *AWCD*, in TAV *vs.* BAV comparisons in subjects with no dilation and stenosis ($TAV_{(-)AS,DIL}$ *vs.* $BAV_{(-)AS,DIL}$), and in subjects presenting only without dilation ($TAV_{(-)DIL}$ *vs.* $BAV_{(-)DIL}$). The results summarized in Fig. 4 suggest that the combination of BAV and AAo dilation concurs to significantly reduce the length of persistence of the large-scale flow coherence in AAo.

This interpretation is corroborated by the fact that *AWCD* in DIL group is significantly shorter than in NoDIL group (Fig. 4, lower panel), regardless of concomitant BAV or AS diseases (0.30 (0.22–0.35) in

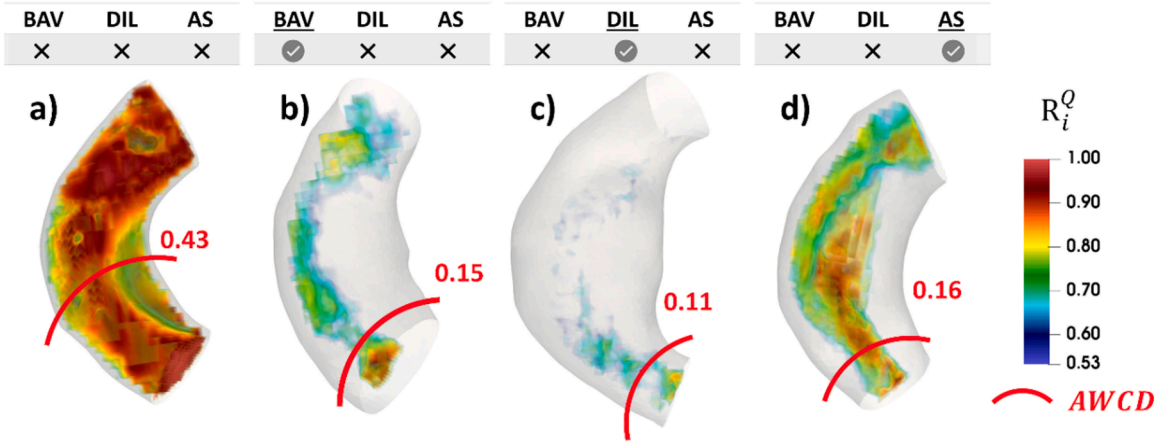

Fig. 3. Volumetric maps of R_i^Q values and *AWCD* values (red line) in AAo in four explanatory cases, namely: (a) one healthy subject and three patients presenting with (b) only BAV, (c) only DIL, and (d) only AS, respectively. Volumetric maps show only R_i^Q values above the cumulative median value $\widehat{R}_i^Q = 0.53$. Reconstructed geometries are shown with different scales.

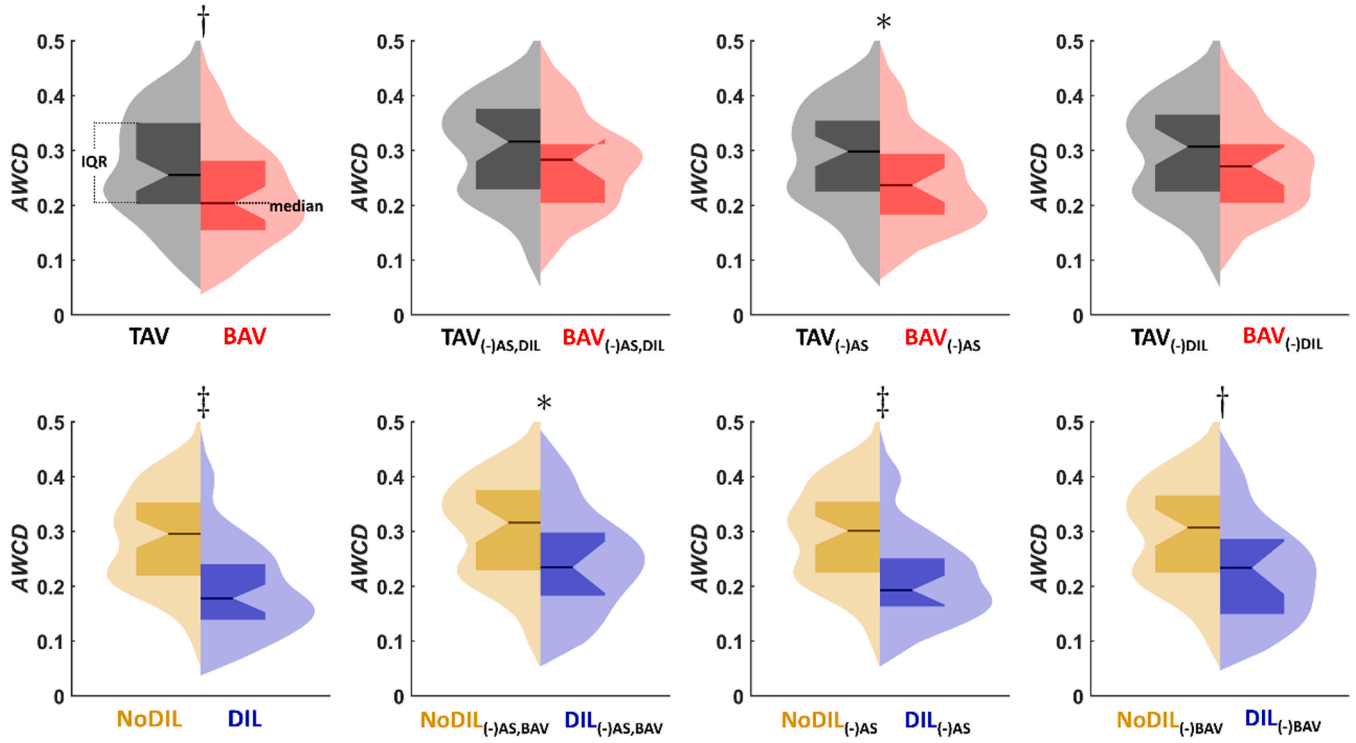

Fig. 4. Violin plots comparing *AWCD* distributions in the TAV *vs.* BAV (upper row) and NoDIL *vs.* DIL (bottom row) groups, and in the respective subgroups accounting for the effects of concomitant pathologies. *AWCD* is normalized by the curvilinear length l_{AAo} of the AAo centerline. In the violin plots, the median is indicated by the black line and the box indicates the interquartile range (IQR). Differences between two groups of patients were assessed using Mann-Whitney U tests. Statistical significance is indicated with: $^{*}p < 0.05$; $^{\dagger}p < 0.01$; $^{\ddagger}p < 0.001$.

NoDIL *vs.* 0.18 (0.14–0.24) in DIL, $p < 0.001$; 0.32 (0.23–0.38) in $\text{NoDIL}_{(-)\text{AS,BAV}}$ subgroup *vs.* 0.23 (0.18–0.30) in $\text{DIL}_{(-)\text{AS,BAV}}$ subgroup, $p < 0.05$; 0.31 (0.22–0.36) in $\text{NoDIL}_{(-)\text{BAV}}$ subgroup *vs.* 0.23 (0.15–0.29) in $\text{DIL}_{(-)\text{BAV}}$ subgroup, $p < 0.01$). Notably, the emerged difference in *AWCD* is more significant when DIL patients present with concomitant BAV (*AWCD* 0.30 (0.22–0.35) in $\text{NoDIL}_{(-)\text{AS}}$ subgroup *vs.* 0.19 (0.16–0.25) in $\text{DIL}_{(-)\text{AS}}$ subgroup, $p < 0.001$).

3.2. Impact of age on large-scale flow coherence

The analysis revealed that *AWCD* is inversely associated with age when considering the entire population (ALL) under study (r=− 0.50, $p < 0.001$), but also isolating TAV subjects (r=− 0.48, $p < 0.01$), BAV patients (r=− 0.52, $p < 0.001$) and NoDIL subjects (r=− 0.42, $p < 0.001$), suggesting that the coherence of the large-scale hemodynamics in terms of similarity with $Q(t)$ at the STJ is lost with age (Fig. 5). From the analyses of the subgroups accounting for the effect of concomitant pathologies, it emerged that the negative associations between *AWCD* and age disappear if no concomitant disease is present (namely, in $\text{TAV}_{(-)\text{AS,DIL}}$, $\text{BAV}_{(-)\text{AS,DIL}}$, and $\text{NoDIL}_{(-)\text{AS,BAV}}$ subgroups, Fig. 5). On the contrary, in DIL patients *AWCD* and age are inversely correlated only in the absence of concomitant diseases (r=− 0.62, $p < 0.05$).

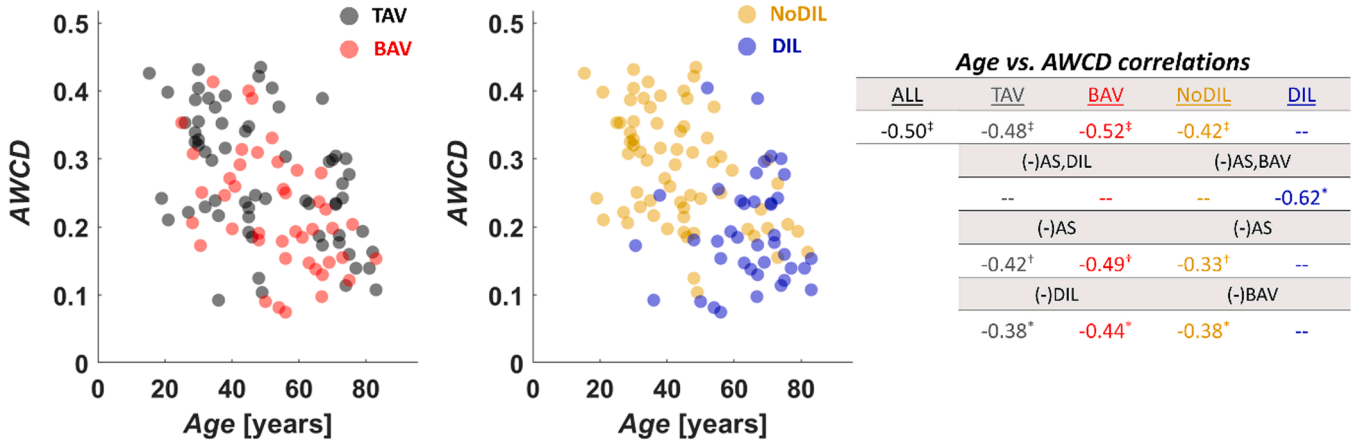

Fig. 5. Scatter plots of *AWCD vs.* age in the entire population (ALL), and in the TAV, BAV, NoDIL and DIL groups (regardless of concomitant pathologies). The corresponding Spearman correlation coefficients are reported in the table on the right, together with the correlation coefficients in the respective subgroups accounting for the effects of concomitant pathologies. *AWCD* is normalized by the curvilinear length l_{AAo} of the AAo centerline. Statistical significance is indicated with: $^{*}p < 0.05$; $^{\dagger}p < 0.01$; $^{\ddagger}p < 0.001$.

3.3. Impact of canonical aortic hemodynamic features and anatomy on large-scale flow coherence

To identify the main determinants of the anatomical length of persistence of AAo flow coherence (expressed in terms of $Q(t)$ *vs.* $V_{ax}(t)$ waveforms similarity), we explored the existence of possible links between *AWCD* and canonical quantities adopted to describe aortic hemodynamics and anatomy. The results of the analysis (age-adjusted when necessary) are summarized in Table 2.

In detail, the analysis revealed that *AWCD* in AAo is positively associated with the average value of the aortic flow rate $\overline{Q}$, and with its peak-to-peak amplitude Q_{p-p}. The association between *AWCD* and $\overline{Q}$ (Table 2 and Fig. 6) is stronger in the DIL and TAV cohorts (r=0.63 and r=0.57, respectively, $p < 0.001$), compared to the NoDIL group (r=0.48, $p < 0.001$). In BAV patients, on the contrary, *AWCD* is not associated with $\overline{Q}$, but it is positively correlated with the AAo peak kinetic energy $\overline{KE}_{peak}$ (r=0.43, $p < 0.01$, Table 2 and Fig. 6). Moreover, *AWCD* is negatively associated with *FJA* when the entire population under study is considered (r=− 0.36, $p < 0.001$), as well as in all the investigated groups with the not surprising exception of TAV subjects, where the aortic flow is not characterized by marked eccentricity. BAV patients presented an association between *AWCD* and *FJA* (r=− 0.54, $p < 0.001$) stronger than NoDIL and DIL cohorts (r=− 0.25 and r=− 0.34, respectively, $p < 0.05$), suggesting that the negative association between the length of persistence of the large-scale flow coherence in AAo and the aortic jet outflow angle is markedly amplified by a coexisting BAV phenotype.

Regarding the aortic anatomic attributes, D_{ratio} and (less markedly) D_{max} present negative associations with *AWCD* (Table 2 and Fig. 6). In particular, D_{ratio} is inversely correlated with *AWCD* in the entire population and in all the investigated groups, with stronger correlations exhibited by BAV and DIL cohorts (r=− 0.79 and r=− 0.75, respectively, $p < 0.001$), compared to TAV and NoDIL (r=− 0.36 and r=− 0.38, respectively, $p < 0.01$). Lastly, an inverse association emerged in BAV patients between the percentage of leaflet fusion %*LF* and *AWCD* (unadjusted r=− 0.43, $p < 0.01$), which lost significance when age-adjusted (Table 2).

3.4. Impact of concomitant pathologies on large-scale flow coherence

To broaden the mechanistic understanding of the coherence of large-scale blood flow in aortic pathophysiology, the impact of concomitant pathologies was investigated. To do that, the nature of the relationship between *AWCD*and the aortic hemodynamics- and anatomy-related features listed in Table 2 for the TAV, BAV, NoDIL and DIL cohorts, was investigated in the subgroups of subjects accounting for the effects of concomitant pathologies (Fig. 7).

It emerged that in general the positive effect of the aortic flow rate $Q(t)$ features on the persistence of large-scale flow coherence in TAV, NoDIL and DIL cohorts (Table 2) is independent of the concomitance of other diseases, and it is confirmed to be stronger in terms of $\overline{Q}$ than in terms of Q_{p-p} (Fig. 7). Similarly, the strong negative correlation between *AWCD* and *FJA* in BAV patients (r=− 0.54, $p < 0.001$, Table 2) is independent of concomitant DIL or AS pathologies (r=− 0.73, $p < 0.001$ in $BAV_{(-)AS,DIL}$ subgroup, r=− 0.66, $p < 0.001$ in $BAV_{(-)AS}$ subgroup, and r=− 0.71, $p < 0.001$ in $BAV_{(-)DIL}$ subgroup, Fig. 7a). To be noted, the inverse association between *AWCD* and *FJA* in the NoDIL cohort (r=− 0.25, $p < 0.05$, Table 2) holds true only in the subgroup of subjects where AS, but not BAV, is excluded (r=− 0.26, $p < 0.05$ in $NoDIL_{(-)AS}$ subgroup, Fig. 7b). These results enforce the hypothesis that BAV phenotype, implying unphysiological flow jet angles, plays a major role in disrupting flow coherence in AAo (as also suggested by the results in Table 2 and Fig. 6).

The positive association between *AWCD* and $\overline{KE}_{peak}$ in the BAV cohort (r=0.43, $p < 0.01$, Table 2, Fig. 6) holds true only in subjects without aortic stenosis, regardless of AAo dilation (r=0.53, $p < 0.05$ and r=0.66, $p < 0.001$ in $BAV_{(-)AS,DIL}$ and $BAV_{(-)AS}$ subgroups, respectively, Fig. 7a). The concomitance of noAS with BAV phenotype is characterized by an *AWCD vs.* $\overline{KE}_{peak}$ positive correlation in both NoDIL (r=0.28, $p < 0.05$ in $NoDIL_{(-)AS}$ subgroup) and DIL (r=0.40, $p < 0.05$ in $DIL_{(-)AS}$ subgroup) subjects (Fig. 7b).

Regarding the link between the length of persistence of AAo flow coherence and aortic anatomic attributes, the emerged strong negative correlation between *AWCD* and D_{ratio} is independent of the presence of concomitant pathologies only in BAV patients (r=− 0.79, $p < 0.001$ in $BAV_{(-)AS,DIL}$ subgroup, r=− 0.86, $p < 0.001$ in $BAV_{(-)AS}$ subgroup, and r=− 0.68, $p < 0.001$ in $BAV_{(-)DIL}$ subgroup, Fig. 7a), whereas in the DIL cohort such negative correlation emerges when AAo dilation is combined with either BAV or AS (r=− 0.68, $p < 0.001$ and r=− 0.70, $p < 0.001$ in $DIL_{(-)AS}$ and $DIL_{(-)BAV}$ subgroups, respectively, Fig. 7b). In TAV subjects, no significant association emerges between *AWCD* and D_{ratio} after removing concomitant pathologies, and in the NoDIL cohort *AWCD* and D_{ratio} are negatively correlated only in subjects with no AS, independent of valve phenotype (r=− 0.38, $p < 0.01$ in $NoDIL_{(-)AS}$ subgroup, Fig. 7b). Lastly, a near significant negative trend emerges between %*LF*

Table 2
Associations of *AWCD* with canonical hemodynamic and anatomic quantities for the entire population under study (ALL), and for the TAV, BAV, NoDIL and DIL cohorts (regardless of concomitant pathologies). Correlations in ALL, TAV, BAV and NoDIL groups are age-adjusted. Statistical significance is indicated with: $*p < 0.05$; $\dagger p < 0.01$; $\ddagger p < 0.001$; –: non-significant; NA: not applicable.

		ALL	TAV	BAV	NoDIL	DIL
Canonical hemodynamic quantities	$\overline{Q}$	$0.47^{\ddagger}$	$0.57^{\ddagger}$	–	$0.48^{\ddagger}$	$0.63^{\ddagger}$
	$Q_{p\text{-}p}$	$0.37^{\ddagger}$	$0.42^{\ddagger}$	0.33*	$0.36^{\dagger}$	$0.70^{\ddagger}$
	Q_{PI}	–	–	–	–	–
	FJA	$-0.36^{\ddagger}$	–	$-0.54^{\ddagger}$	−0.25*	−0.34*
	FD	$-0.29^{\dagger}$	–	–	$-0.38^{\dagger}$	–
	V_{max}	–	–	–	–	–
	$\overline{KE}_{avg}$	–	−0.25*	–	–	–
	$\overline{KE}_{peak}$	–	–	$0.43^{\dagger}$	–	–
Geometric quantities	D_{max}	$-0.41^{\ddagger}$	–	$-0.66^{\ddagger}$	−0.30*	–
	D_{root}	–	–	–	–	$0.60^{\ddagger}$
	D_{ratio}	$-0.58^{\ddagger}$	$-0.36^{\dagger}$	$-0.79^{\ddagger}$	$-0.38^{\dagger}$	$-0.75^{\ddagger}$
	$\overline{\kappa}$	–	–	–	–	–
	$\overline{\tau}$	–	–	–	–	–
	H	–	–	–	–	–
	W	–	–	–	–	–
	H/W	–	–	–	–	–
	%LF	NA	NA	–	NA	–

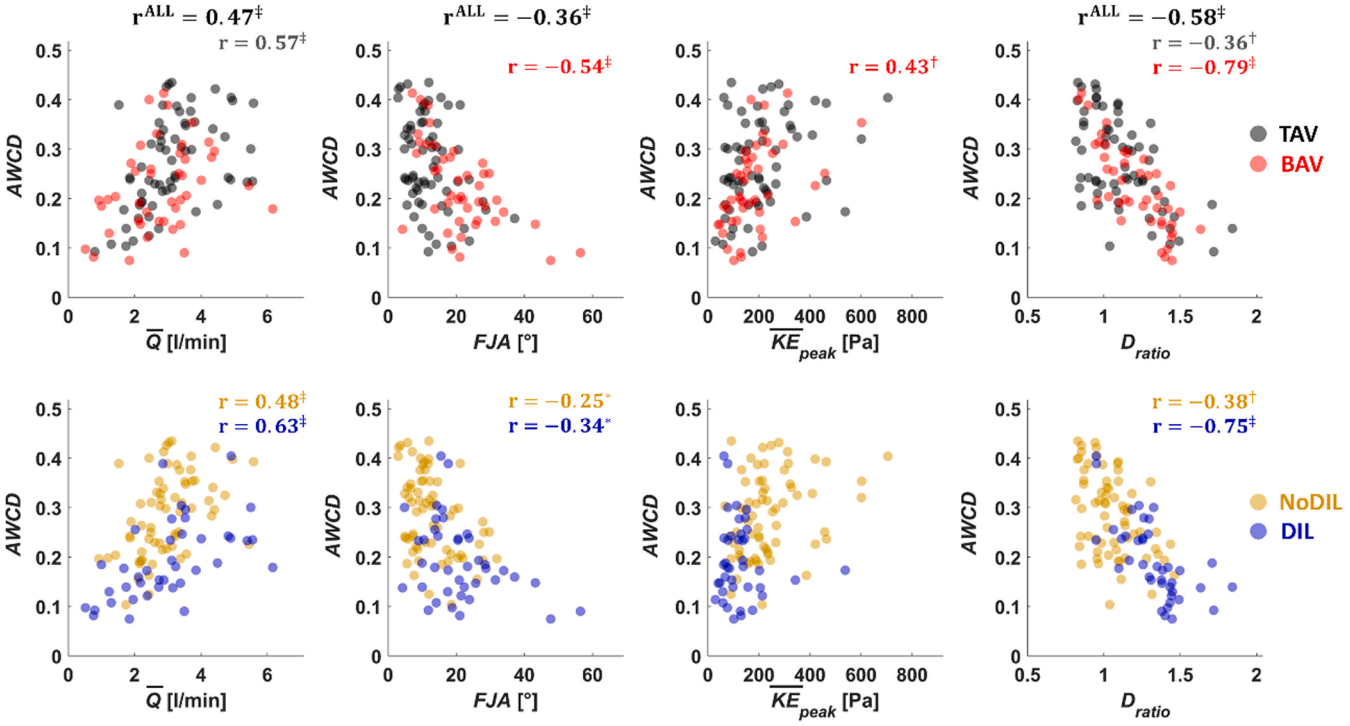

Fig. 6. Scatter plots of *AWCD vs.* $\overline{Q}$ (first column), *FJA* (second column), $\overline{KE}_{peak}$ (third column) and D_{ratio} (fourth column) in the entire population (ALL), and in the TAV, BAV, NoDIL and DIL groups (regardless of concomitant pathologies). The corresponding Spearman correlation coefficients r are also reported. *AWCD* was normalized with respect to the curvilinear length l_{AAo} of the AAo centerline. Statistical significance is indicated with: $^*p < 0.05$; $\dagger p < 0.01$; $\ddagger p < 0.001$.

and *AWCD* in BAV patients with no other concomitant diseases (r=− 0.46, $p = 0.060$ in $BAV_{(-)AS,DIL}$ subgroup, Fig. 7a) and in BAV patients presenting without AS or DIL (r=− 0.38, $p = 0.052$ and r=− 0.41, $p = 0.069$ in $BAV_{(-)AS}$ and $BAV_{(-)DIL}$ subgroups, respectively, Fig. 7a).

4. Discussion

The onset and progression of aortic disorders reflect a complex interplay between multiple factors. Among them, hemodynamics has been proven to be markedly involved [24,18,52,6,54,55]. However, to provide risk stratification tools that meet clinical requirements, many studies look at aortic flows at single time points or use spatiotemporally averaged quantities, driven by the need of implementing a reductionist approach to face the complex nature of aortic hemodynamics [56–58]. By studying the spatiotemporal similarity of arterial flow waveforms, an approach based on network science [24,31–35] has recently offered a different picture of the relationship between blood flow and arterial pathophysiology, that cannot emerge from the canonical hemodynamic analysis. Technically, the so called *"one-to-all"* network approach [31] was proposed to investigate the role of blood flow rate $Q(t)$ waveform at the AAo inflow in the forward flow coherence and to quantify the anatomical length of persistence of such coherent motion. The *"one-to-all"* analysis was recently applied to 4D flow MRI data of healthy subjects, allowing to quantitatively determine distinguishable hemodynamic features of coherent large-scale aortic fluid motion [34]. By using the latter as physiological reference framework, the present study extends the *"one-to-all"* network approach to a large and stratified dataset of thoracic aortas with the aim of: (1) evaluating how blood flow physiological coherence is disrupted by AAo dilation and BAV phenotype; (2) identifying those hemodynamic and anatomic features playing a role in either preserving or disrupting AAo flow coherence; and (3) assessing the effects of concomitant AAo dilation and valve dysfunction on the anatomic length of persistence *AWCD* of blood flow coherence when advected to the distal AAo.

The main findings of this study (Fig. 8) are: (1) *AWCD* is maximum in the healthy aorta (43 % of the AAo curvilinear length, Fig. 3a), and is significantly shortened in the presence of BAV and AS (15 % and 16 %, respectively, Fig. 3b and 3d), and even more in a dilated AAo (down to 11 % of l_{AAo}, Fig. 3c); (2) the AAo canonical hemodynamic features and anatomic attributes with the strongest association with *AWCD* are the cycle-average STJ blood flow rate $\overline{Q}$ (except in BAV patients) and the AAo dilation as measured by D_{ratio}, which act in opposite directions to promote and hamper, respectively, the persistence of AAo forward flow coherence; (3) the influence of $\overline{Q}$ and of D_{ratio} on *AWCD* is independent of concomitant BAV, DIL or AS pathologies, respectively in every cohort and only in the BAV group.

4.1. Large-scale flow coherence and aortic disease

In healthy subjects, a remarkable dynamical similarity (high R_i^Q values) between the forward flow and the flow rate waveform at STJ characterizes in general the entire AAo volume (Fig. 3a), despite the recognized physiological intersubject variability [34]. The disruption of AAo flow coherence, and the consequent reduction of its anatomical length of persistence in the non-healthy aorta can be explained in terms of establishment of flow separation and recirculation patterns as a consequence of the combined effect of AAo curvature and (eccentric) aortic outflow jet in BAV and AS patients [59,60], and of the aortic expansion in DIL patients [14,61]. Such flow disturbances are in fact characterized by the presence of retrograde flow, identified by negative $V_{ax}(t)$ [33], which are inversely correlated with the aortic blood flow rate $Q(t)$ driving the forward flow [34]. Interestingly, it emerged that *AWCD* in BAV is shorter than TAV only if the BAV is associated with a dilated AAo (Fig. 4, upper panel), suggesting that the sole BAV per se may not be able to significantly disrupt AAo flow coherence, which only occurs when the valve-mediated impaired hemodynamics is exacerbated by wall dilation. This finding is in agreement with previous *in silico* and *in vivo* studies demonstrating that a surgical repair of tubular AAo with preservation of the native BAV allowed to restore a positive

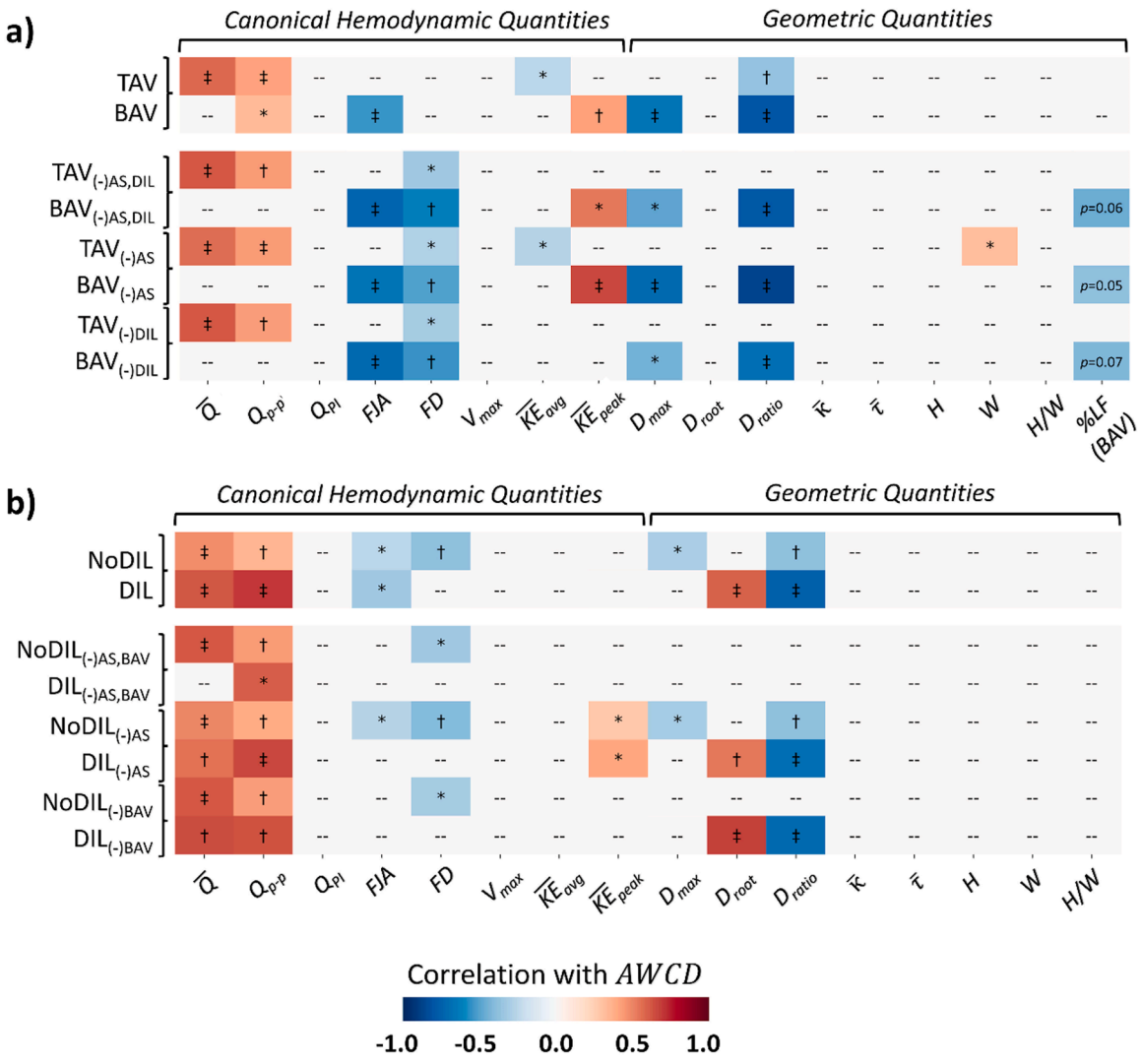

Fig. 7. Colormaps of the Spearman correlation coefficients between *AWCD* and the aortic hemodynamics- and anatomy-related features listed in Table 2, in the TAV and BAV groups (panel a)), and in the NoDIL and DIL groups (panel b)), as well as in the respective subgroups accounting for the effects of concomitant pathologies. Statistical significance is indicated with: $*p < 0.05$; $\dagger p < 0.01$; $\ddagger p < 0.001$.

hemodynamic environment, by partially suppressing flow recirculation, aortic valve flow jet impingement on the AAo wall and viscous energy losses [23], as well as by inducing a more physiological helical flow [62, 63]. Only investigating longitudinal data would allow us to clarify whether the disruption of hemodynamic coherence in BAV patients is involved in the progression of AAo dilation. Based on our findings we can only state that, in BAV patients, dilation contributes to the disruption of AAo flow coherence, which is expected to be the hallmark of the presence of flow disturbances advected through the aorta, more markedly than in TAV patients.

4.2. Hemodynamic and anatomic factors determining AAo flow coherence

The age-adjusted correlation analyses revealed that the STJ blood flow rate, in particular the average blood flow rate $\overline{Q}$ (and, to a lesser extent, the peak-to-peak amplitude Q_{p-p}) is the hemodynamic feature with the strongest influence on the persistence length of coherence in large-scale flow in AAo (*AWCD vs.* $\overline{Q}$: r =0.49 in the entire population, $p < 0.001$, Table 2 and Fig. 6). This finding suggests that inertial forces significantly contribute to preserve the hemodynamic coherence along the healthy thoracic aorta [34]. The importance of the proximal AAo blood flow rate waveform in shaping the distal aortic hemodynamics was also highlighted by previous 4D flow MRI studies reporting that aortic flow rate (measured in terms of stroke volume or cardiac output) remarkably impacts on flow velocity and vorticity in healthy subjects [64], and on wall shear stress (WSS) and systolic helicity also in younger subjects [65].

By extending the investigation to diseased aortas, this study further demonstrates that, except for the BAV cohort (*AWCD vs.* $\overline{Q}$: r=0.27, $p = 0.09$), higher cycle-average flow rates promote AAo large-scale flow coherence also in the TAV, NoDIL and DIL cohorts (*AWCD vs.* $\overline{Q}$: r=0.63, r=0.48 and r=0.57, respectively, $p < 0.001$, Table 2 and Fig. 6).

Along with the average blood flow rate $\overline{Q}$, the AAo diameter enlargement as measured by D_{ratio} has emerged as a main factor determining the length of persistence of AAo hemodynamic coherence. A previous study on a smaller and less stratified 4D flow MRI dataset of dilated and non-dilated aortas (mainly patients with moderate-to-severe TAV dysfunction) suggested that high D_{ratio} values might disrupt the large-scale blood flow coherence, reducing the persistence length of the correlation among $V_{ax}(t)$ waveforms [33]. The *"one-to-all"* analysis in the present study extends this role for D_{ratio} also to the spatiotemporal similarity between $V_{ax}(t)$ waveforms and the proximal blood flow rate $Q(t)$ (*AWCD vs.* D_{ratio}: r=− 0.59 in the entire population, $p < 0.001$,

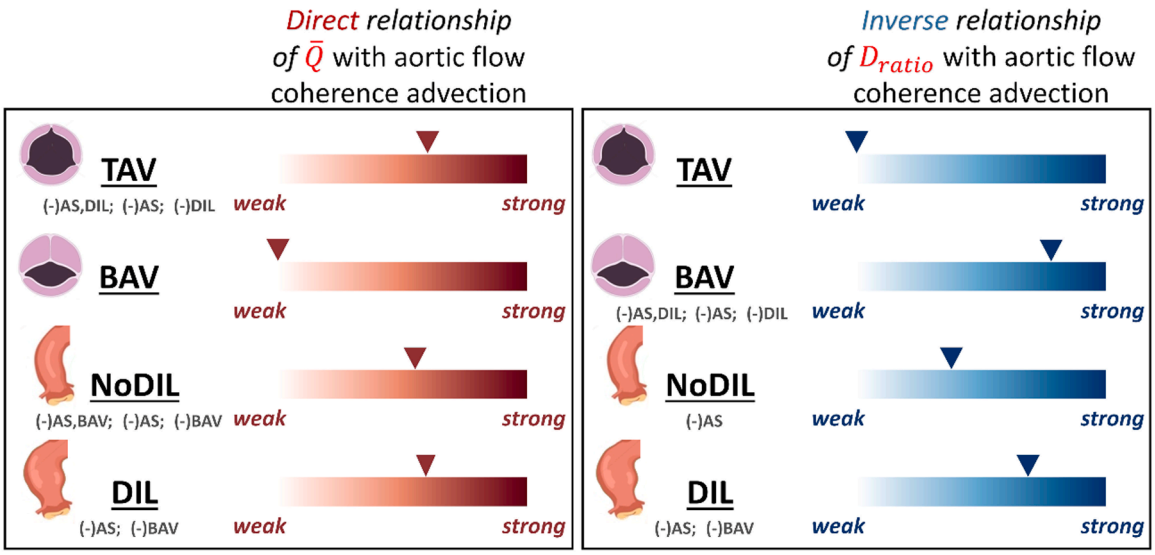

Fig. 8. Summary of the main findings on the impact of *AWCD*'s main determinants, accounting for concomitant pathologies. Left panel: the red color bars represent the strength of the direct relationship of $\overline{Q}$ with the aortic flow coherence advection (as measured in terms of $\overline{Q}$ *vs. AWCD* positive correlations). Right panel: the blue color bars represent the strength of the inverse relationship of D_{ratio} with the aortic flow coherence advection (as measured in terms of D_{ratio} *vs. AWCD* negative correlations).

Table 2 and Fig. 6). The detrimental effect of an increasing D_{ratio} on the preservation of large-scale flow coherence can be ascribed to the fact that a sudden vessel enlargement predisposes to the production of more heterogeneous fluid structures being associated to the establishment of regions of flow separation and recirculation, and supraphysiological vortical and helical flow patterns, as previously reported [23,28,30,61,66,67].

4.3. Combined effect of aortic dilation and valve dysfunction on the persistence of flow coherence

When accounting for the combined effect of AAo dilation (DIL) and aortic valve morphology and dysfunction (AS), the findings from this study show that blood flow rate $\overline{Q}$ exerts its dominant positive effect on the persistence of large-scale forward flow coherence irrespective of concomitant pathologies (Fig. 7a and 7b). On the contrary, the detrimental action of D_{ratio} on *AWCD* is independent of concomitant DIL or AS only in patients with a BAV (r=− 0.79, $p < 0.001$ in $BAV_{(-)AS,DIL}$ subgroup, r=− 0.86, $p < 0.001$ in $BAV_{(-)AS}$ subgroup, and r=− 0.68, $p < 0.001$ in $BAV_{(-)DIL}$ subgroup, Fig. 7a), whereas it depends on the presence of AS or BAV both in patients with non-dilated AAo (r=− 0.38, $p < 0.01$ in $NoDIL_{(-)AS}$ subgroup, Fig. 7b) and with dilated AAo (r=− 0.68, $p < 0.001$ and r=− 0.70, $p < 0.001$ in $DIL_{(-)AS}$ and $DIL_{(-)BAV}$ subgroups, respectively, Fig. 7b). The stronger detrimental impact of D_{ratio} on the extent of the length of persistence of forward flow coherence in BAV compared to DIL patients (characterized by higher D_{ratio} values, $p < 0.02$), can be explained by the concomitant action of the BAV eccentric systolic outflow jet (high *FJA*) in producing abnormal helical flow [56,68,69]. In this study, in fact, the negative associations emerged between *FJA* and *AWCD* were independent of concomitant diseases only in BAV (r=− 0.73, $p < 0.001$ in $BAV_{(-)AS,DIL}$ subgroup, r=− 0.66, $p < 0.001$ in $BAV_{(-)AS}$ subgroup, and r=− 0.71, $p < 0.001$ in $BAV_{(-)DIL}$ subgroup, Fig. 7a). On the contrary, no association emerged between *FJA* and *AWCD* in TAV subjects (r=− 0.11, $p = 0.40$), while they were negatively associated in NoDIL and DIL subjects only when BAV patients were considered (r=− 0.25 and r=− 0.34, in NoDIL and DIL groups respectively, $p < 0.05$; r=− 0.26, $p < 0.05$ in $NoDIL_{(-)AS}$ subgroup, Fig. 7b). These findings suggest that the flow eccentricity characterizing the BAV hemodynamics may be the factor responsible (albeit to a small extent, as suggested by the emerged weak-to-moderate correlations) for the disruption of AAo flow coherence, irrespectively of dilation and AS. This is corroborated by previous studies reporting of a supraphysiological AAo systolic helical flow correlated with the eccentric systolic outflow jet in BAV patients (with or without DIL or AS), which does not develop in healthy TAV subjects or in TAV patients with DIL and/or AS [56,68,69]. Moreover, adding clinical relevance to the present findings, it was demonstrated that the combined action of AAo dilation and flow eccentricity in promoting an adverse hemodynamics in BAV patients is associated with markedly asymmetric WSS patterns in the AAo [30,66,70,71], an hallmark of risk of vascular injury and aneurysm formation/growth [6,72,73].

5. Limitations

This study suffers from limitations that might weaken its findings. Among the main limitations we mention the noise affecting the 4D flow MRI data, which could potentially lead to underestimate the correlation between $Q(t)$ and $V_{ax}(t)$ waveforms. However, as such correlation is predominantly driven by the waveform shapes along the systolic phase, which is characterized by a higher signal-to-noise ratio than the diastolic phase, the impact of noise in the obtained results can be considered marginal. Another limitation is the cross-sectional nature of this investigation. Longitudinal studies on follow-up data are in fact needed to confirm the present findings on the impact of aortic disease on large-scale flow coherence and to draw any clinically relevant conclusion on the effectiveness of the *AWCD* network metric as an *in vivo* risk prediction tool. Finally, in this study the investigation of the aortic flow coherence is focused on the large scales of the aortic flow. In the future, the network-based analysis could be expanded to include the evaluation of coherence of the small-scale aortic hemodynamics.

6. Conclusions

This study enriches the evidence on the potential of the network-based approach in identifying large-scale flow coherence also in the presence of aortic disease, demonstrating that the presence of AAo dilation as well as of BAV phenotype breaks the physiological aortic flow coherence. Moreover, it emerged that high average aortic blood flow rates generally concur to preserve flow coherence, both in healthy and diseased aortas, whereas an increasing AAo dilation exacerbates the

flow coherence disruption, especially in patients with a concomitant BAV. The encouraging findings regarding the ability of the network approach in discriminating between healthy and diseased AAo blood flow coherence may pave the way for future longitudinal studies, which are necessary to provide effective clinical relevance. Follow-up investigations could be performed to verify the role of the anatomical persistence length of flow coherence in the progression of aortic disease (*e.g.*, AAo dilation or BAV condition) and to identify risk-associated objective *AWCD* thresholds which, alone or in combination with aortic anatomic attributes, may support (i) a more effective patients' risk stratification, (ii) the prediction of specific disease trajectories, (iii) the evaluation of pharmacological and/or surgical treatments (*e.g.* BAV repair or replacement) in the restoration of the physiological hemodynamics (in terms of aortic flow coherence), and (iv) the design and optimization of surgical procedures and implantable cardiovascular devices. The network-based approach adopted in this study can be easily integrated into a 4D flow MRI clinical framework to enrich the arsenal of tools for the *in vivo* non-invasive assessment of risk associated with the onset and progression of aortic diseases.

CRediT authorship contribution statement

Karol Calò: Writing – review & editing, Writing – original draft, Visualization, Software, Methodology, Investigation, Formal analysis, Data curation, Conceptualization. **Andrea Guala:** Writing – review & editing, Resources, Investigation, Funding acquisition, Data curation, Conceptualization. **Valentina Mazzi:** Writing – review & editing, Visualization, Formal analysis. **Maurizio Lodi Rizzini:** Writing – review & editing, Software, Formal analysis. **Lydia Dux-Santoy:** Writing – review & editing, Investigation, Data curation. **Jose Rodriguez-Palomares:** Resources, Investigation. **Stefania Scarsoglio:** Writing – review & editing, Methodology. **Luca Ridolfi:** Writing – review & editing, Methodology. **Diego Gallo:** Writing – review & editing, Writing – original draft, Supervision, Resources, Methodology, Funding acquisition, Conceptualization. **Umberto Morbiducci:** Writing – review & editing, Writing – original draft, Supervision, Resources, Methodology, Funding acquisition, Formal analysis, Conceptualization.

Declaration of competing interest

The authors declare that they have no known competing financial interests or personal relationships that could have appeared to influence the work reported in this paper.

Acknowledgments

The authors K.C., D.G. and U.M. acknowledge the support of «ASSOCIATE» project (code 2022L7KK7L) – funded by European Union – Next Generation EU within the PRIN 2022 program (D.D. 104 - 02/02/2022 Ministero dell'Università e della Ricerca). Author A.G. has received funding from "la Caixa" Foundation (LCF/BQ/PR22/11920008).

References

[1] A. Evangelista, E.M. Isselbacher, E. Bossone, T.G. Gleason, M.Di Eusanio, U. Sechtem, M.P. Ehrlich, S. Trimarchi, A.C. Braverman, T. Myrmel, et al., Insights from the international registry of acute aortic dissection: a 20-year experience of collaborative clinical research, Circulation 137 (2018) 1846–1860, https://doi.org/10.1161/CIRCULATIONAHA.117.031264.

[2] G.A. Roth, D. Abate, K.H. Abate, S.M. Abay, C. Abbafati, N. Abbasi, H. Abbastabar, F. Abd-Allah, J. Abdela, A. Abdelalim, et al., Global, regional, and national age-sex-specific mortality for 282 causes of death in 195 countries and territories, 1980–2017: a systematic analysis for the Global Burden of Disease Study 2017, Lancet 392 (2018) 1736–1788, https://doi.org/10.1016/S0140-6736(18)32203-7.

[3] R. Erbel, V. Aboyans, C. Boileau, E. Bossone, R.Di Bartolomeo, H. Eggebrecht, A. Evangelista, V. Falk, H. Frank, O. Gaemperli, et al., 2014 ESC Guidelines on the diagnosis and treatment of aortic diseases: document covering acute and chronic aortic diseases of the thoracic and abdominal aorta of the adult. The task force for the diagnosis and treatment of aortic diseases of the European, Eur. Heart. J. 35 (2014) 2873–2926, https://doi.org/10.1093/eurheartj/ehu281.

[4] J.A. Elefteriades, E.A. Farkas, Thoracic aortic aneurysm clinically pertinent controversies and uncertainties, J. Am. Coll. Cardiol. 55 (2010) 841–857, https://doi.org/10.1016/j.jacc.2009.08.084.

[5] S. Verma, S.C. Siu, Aortic dilatation in patients with bicuspid aortic valve, N. Engl. J. Med. 370 (2014) 1920–1929, https://doi.org/10.1056/NEJMra1207059.

[6] A. Guala, L. Dux-Santoy, G. Teixido-Tura, A. Ruiz-Muñoz, L. Galian-Gay, M. L. Servato, F. Valente, L. Gutiérrez, T. González-Alujas, K.M. Johnson, et al., Wall shear stress predicts aortic dilation in patients with bicuspid aortic valve, JACC Cardiovasc. ImAging 15 (2022) 46–56, https://doi.org/10.1016/j.jcmg.2021.09.023.

[7] J.F. Rodríguez-Palomares, L. Dux-Santoy, A. Guala, L. Galian-Gay, A. Evangelista, Mechanisms of aortic dilation in patients with bicuspid aortic valve, J. Am. Coll. Cardiol. 82 (2023) 448–464, https://doi.org/10.1016/j.jacc.2022.10.042.

[8] E. Bossone, K.A. Eagle, Epidemiology and management of aortic disease: aortic aneurysms and acute aortic syndromes, Nat. Rev. Cardiol. 18 (2021) 331–348, https://doi.org/10.1038/s41569-020-00472-6.

[9] A.A. Hardikar, T.H. Marwick, The natural history of guidelines: the case of aortopathy related to bicuspid aortic valves, Int. J. Cardiol. 199 (2015) 150–153, https://doi.org/10.1016/j.ijcard.2015.06.059.

[10] M.Y. Salmasi, S. Alwis, S. Cyclewala, O.A. Jarral, H. Mohamed, D. Mozalbat, C. A. Nienaber, T. Athanasiou, D. Morris-Rosendahl, J. Moore Jr, et al., The genetic basis of thoracic aortic disease: the future of aneurysm classification? Hell. J. Cardiol. 69 (2023) 41–50, https://doi.org/10.1016/j.hjc.2022.09.009.

[11] V. Raghav, A.J. Barker, D. Mangiameli, L. Mirabella, M. Markl, A.P. Yoganathan, Valve mediated hemodynamics and their association with distal ascending aortic diameter in bicuspid aortic valve subjects, J. Magn. Reson. Imaging 47 (2018) 246–254, https://doi.org/10.1002/jmri.25719.

[12] F. Hammareus, C. Trenti, H.M. Bjorck, J. Engvall, P. Eriksson, H. Lekedal, A. Lundberg, L. Nilsson, E. Swahn, L. Jonasson, et al., Hemodynamics and plasma biomarkers in individuals with mild-to-moderate ascending aortic dilatation and tricuspid aortic valves, Eur. Heart. J. 44 (2023), https://doi.org/10.1093/eurheartj/ehad655.2030.

[13] M. Salmasi, O. Jarral, S. Pirola, S. Sasidharan, J. Pepper, A. Oo, J. Moore Jr, X. Xu, T. Athanasiou, *In-vivo* blood flow parameters can predict at-risk aortic aneurysms and dissection: a comprehensive biomechanics model, Eur. Heart. J. 41 (2020), https://doi.org/10.1093/ehjci/ehaa946.2339 ehaa946-2339.

[14] J. Burk, P. Blanke, Z. Stankovic, A. Barker, M. Russe, J. Geiger, A. Frydrychowicz, M. Langer, M. Markl, Evaluation of 3D blood flow patterns and wall shear stress in the normal and dilated thoracic aorta using flow-sensitive 4D CMR, J. Cardiovasc. Magn. Reson. 14 (2012) 84, https://doi.org/10.1186/1532-429X-14-84.

[15] K. Suwa, O.A. Rahman, E. Bollache, M.J. Rose, A.A. Rahsepar, J.C. Carr, J. D. Collins, A.J. Barker, M. Markl, Effect of aortic valve disease on 3D hemodynamics in patients with aortic dilation and trileaflet aortic valve morphology, J. Magn. Reson. Imaging 51 (2020) 481–491, https://doi.org/10.1002/jmri.26804.

[16] R. Mahadevia, A.J. Barker, S. Schnell, P. Entezari, P. Kansal, P.W.M. Fedak, S. C. Malaisrie, P. McCarthy, J. Collins, J. Carr, et al., Bicuspid aortic cusp fusion morphology alters aortic three-dimensional outflow patterns, wall shear stress, and expression of aortopathy, Circulation 129 (2014) 673–682, https://doi.org/10.1161/CIRCULATIONAHA.113.003026.

[17] E. Bollache, D.G. Guzzardi, S. Sattari, K.E. Olsen, E.S. Di Martino, S.C. Malaisrie, P. van Ooij, J. Collins, J. Carr, P.M. McCarthy, et al., Aortic valve-mediated wall shear stress is heterogeneous and predicts regional aortic elastic fiber thinning in bicuspid aortic valve-associated aortopathy, J. Thorac. Cardiovasc. Surg. 156 (2018), https://doi.org/10.1016/j.jtcvs.2018.05.095, 2112-2120.e2.

[18] S. Pasta, V. Agnese, A. Gallo, F. Cosentino, M. Di Giuseppe, G. Gentile, G.M. Raffa, J.F. Maalouf, H.I. Michelena, D. Bellavia, Shear stress and aortic strain associations with biomarkers of ascending thoracic aortic aneurysm, Ann. Thorac. Surg. 110 (2020) 1595–1604, https://doi.org/10.1016/j.athoracsur.2020.03.017.

[19] P. Corso, D. Obrist, On the role of aortic valve architecture for physiological hemodynamics and valve replacement, Part I: flow configuration and vortex dynamics, Comput. Biol. Med. 176 (2024) 108526, https://doi.org/10.1016/j.compbiomed.2024.108526.

[20] A. Olcay, A. Amindari, K. Kirkkopru, H. Yalcin, Characterization of disturbed hemodynamics due to Stenosed aortic jets with a Lagrangian coherent structures technique, J. Appl. Fluid Mech. 11 (2018) 375–384, https://doi.org/10.29252/jafm.11.02.28185.

[21] P. Corso, U. Gülan, N. Cohrs, W.J. Stark, F. Duru, M. Holzner, Comprehensive *in vitro* study of the flow past two transcatheter aortic valves: comparison with a severe stenotic case, Ann. Biomed. Eng. 47 (2019) 2241–2257, https://doi.org/10.1007/s10439-019-02289-y).

[22] P. Corso, D. Obrist, On the role of aortic valve architecture for physiological hemodynamics and valve replacement, Part II: spectral analysis and anisotropy, Comput. Biol. Med. 176 (2024) 108552, https://doi.org/10.1016/j.compbiomed.2024.108552.

[23] F. Condemi, S. Campisi, M. Viallon, P. Croisille, J.-F. Fuzelier, S. Avril, Ascending thoracic aorta aneurysm repair induces positive hemodynamic outcomes in a patient with unchanged bicuspid aortic valve, J. Biomech. 81 (2018) 145–148, https://doi.org/10.1016/j.jbiomech.2018.09.022.

[24] G. De Nisco, P. Tasso, K. Calò, V. Mazzi, D. Gallo, F. Condemi, S. Farzaneh, S. Avril, U. Morbiducci, Deciphering ascending thoracic aortic aneurysm hemodynamics in relation to biomechanical properties, Med. Eng. Phys. 82 (2020) 119–129, https://doi.org/10.1016/j.medengphy.2020.07.003.

[25] M.Y. Salmasi, S. Pirola, S. Sasidharan, S.M. Fisichella, A. Redaelli, O.A. Jarral, D. P. O'Regan, A.Y. Oo, J.E. Moore, X.Y. Xu, et al., High wall shear stress can predict wall degradation in ascending aortic aneurysms: an integrated biomechanics study, Front. Bioeng. Biotechnol. 9 (2021), https://doi.org/10.3389/fbioe.2021.750656.
[26] P. Youssefi, A. Gomez, T. He, L. Anderson, N. Bunce, R. Sharma, C.A. Figueroa, M. Jahangiri, Patient-specific computational fluid dynamics-assessment of aortic hemodynamics in a spectrum of aortic valve pathologies, J. Thorac. Cardiovasc. Surg. 153 (2017), https://doi.org/10.1016/j.jtcvs.2016.09.040, 8-20.e3.
[27] P. Youssefi, A. Gomez, C. Arthurs, R. Sharma, M. Jahangiri, C. Alberto Figueroa, Impact of patient-specific inflow velocity profile on hemodynamics of the thoracic aorta, J. Biomech. Eng. 140 (2017), https://doi.org/10.1115/1.4037857.
[28] R. Jayendiran, S. Campisi, M. Viallon, P. Croisille, S. Avril, Hemodynamics alteration in patient-specific dilated ascending thoracic aortas with tricuspid and bicuspid aortic valves, J. Biomech. 110 (2020) 109954, https://doi.org/10.1016/j.jbiomech.2020.109954.
[29] J. Sotelo, P. Franco, A. Guala, L. Dux-Santoy, A. Ruiz-Muñoz, A. Evangelista, H. Mella, J. Mura, D.E. Hurtado, J.F. Rodríguez-Palomares, et al., Fully three-dimensional hemodynamic characterization of altered blood flow in bicuspid aortic valve patients with respect to aortic dilatation: a finite element approach, Front. Cardiovasc. Med. 9 (2022), https://doi.org/10.3389/fcvm.2022.885338.
[30] J.F. Rodríguez-Palomares, L. Dux-Santoy, A. Guala, R. Kale, G. Maldonado, G. Teixidó-Turà, L. Galian, M. Huguet, F. Valente, L. Gutiérrez, et al., Aortic flow patterns and wall shear stress maps by 4D-flow cardiovascular magnetic resonance in the assessment of aortic dilatation in bicuspid aortic valve disease, J. Cardiovasc. Magn. Reson. 20 (2018) 28, https://doi.org/10.1186/s12968-018-0451-1.
[31] K. Calò, D. Gallo, D.A. Steinman, V. Mazzi, S. Scarsoglio, L. Ridolfi, U. Morbiducci, Spatiotemporal hemodynamic complexity in carotid arteries: an integrated computational hemodynamics & complex networks-based approach, IEEE Trans. Biomed. Eng. 67 (2020) 1841–1853, https://doi.org/10.1109/TBME.2019.2949148.
[32] K. Calò, G. De Nisco, D. Gallo, C. Chiastra, A. Hoogendoorn, D.A. Steinman, S. Scarsoglio, J.J. Wentzel, U. Morbiducci, Exploring wall shear stress spatiotemporal heterogeneity in coronary arteries combining correlation-based analysis and complex networks with computational hemodynamics, Proc. Inst. Mech. Eng. Part H J. Eng. Med. 234 (2020) 1209–1222, https://doi.org/10.1177/0954411920923253.
[33] K. Calò, D. Gallo, A. Guala, J. Rodriguez Palomares, S. Scarsoglio, L. Ridolfi, U. Morbiducci, Combining 4D flow MRI and complex networks theory to characterize the hemodynamic heterogeneity in dilated and non-dilated human ascending aortas, Ann. Biomed. Eng. 49 (2021) 2441–2453, https://doi.org/10.1007/s10439-021-02798-9.
[34] K. Calò, D. Gallo, A. Guala, M.L. Rizzini, L. Dux-Santoy, J. Rodriguez-Palomares, S. Scarsoglio, L. Ridolfi, U. Morbiducci, Network-based characterization of blood large-scale coherent motion in the healthy human aorta with 4D flow MRI, IEEE Trans. Biomed. Eng. 70 (2023) 1095–1104, https://doi.org/10.1109/TBME.2022.3209736.
[35] K. Calò, K. Capellini, G. De Nisco, V. Mazzi, E. Gasparotti, D. Gallo, S. Celi, U. Morbiducci, Impact of wall displacements on the large-scale flow coherence in ascending aorta, J. Biomech. 154 (2023) 111620, https://doi.org/10.1016/j.jbiomech.2023.111620.
[36] P. Youssefi, A. Gomez, C. Arthurs, R. Sharma, M. Jahangiri, C. Alberto Figueroa, Impact of patient-specific inflow velocity profile on hemodynamics of the thoracic aorta, J. Biomech. Eng. 140 (2018), https://doi.org/10.1115/1.4037857.
[37] U. Morbiducci, R. Ponzini, D. Gallo, C. Bignardi, G. Rizzo, Inflow boundary conditions for image-based computational hemodynamics: impact of idealized *versus* measured velocity profiles in the human aorta, J. Biomech. 46 (2013) 102–109, https://doi.org/10.1016/j.jbiomech.2012.10.012.
[38] L. Campens, L. Demulier, K. De Groote, K. Vandekerckhove, D. De Wolf, M. J. Roman, R.B. Devereux, A. De Paepe, J. De Backer, Reference values for echocardiographic assessment of the diameter of the aortic root and ascending aorta spanning all age categories, Am. J. Cardiol. 114 (2014) 914–920, https://doi.org/10.1016/j.amjcard.2014.06.024.
[39] C.M. Otto, R.A. Nishimura, R.O. Bonow, B.A. Carabello, J.P. Erwin, F. Gentile, H. Jneid, E.V. Krieger, M. Mack, C. McLeod, et al., 2020 ACC/AHA guideline for the management of patients with valvular heart disease: a report of the American College of Cardiology/American Heart Association Joint Committee on Clinical Practice Guidelines, Circulation 143 (2021) e72–e227, https://doi.org/10.1161/CIR.0000000000000923.
[40] K.M. Johnson, D.P. Lum, P.A. Turski, W.F. Block, C.A. Mistretta, O. Wieben, Improved 3D phase contrast MRI with off-resonance corrected dual echo VIPR, Magn. Reson. Med. 60 (2008) 1329–1336, https://doi.org/10.1002/mrm.21763.
[41] U. Morbiducci, D. Gallo, S. Cristofanelli, R. Ponzini, M.A. Deriu, G. Rizzo, D. A. Steinman, A rational approach to defining principal axes of multidirectional wall shear stress in realistic vascular geometries, with application to the study of the influence of helical flow on wall shear stress directionality in aorta, J. Biomech. 48 (2015) 899–906, https://doi.org/10.1016/j.jbiomech.2015.02.027.
[42] M. Sigovan, M.D. Hope, P. Dyverfeldt, D. Saloner, Comparison of four-dimensional flow parameters for quantification of flow eccentricity in the ascending aorta, J. Magn. Reson. Imaging 34 (2011) 1226–1230, https://doi.org/10.1002/jmri.22800.
[43] M. Friedman, O. Deters, F. Mark, C. Brentbargeron, G. Hutchins, Arterial geometry affects hemodynamics *1A potential risk factor for atherosclerosis, Atherosclerosis 46 (1983) 225–231, https://doi.org/10.1016/0021-9150(83)90113-2).
[44] P. Ou, D.S. Celermajer, O. Raisky, O. Jolivet, F. Buyens, A. Herment, D. Sidi, D. Bonnet, E. Mousseaux, Angular (Gothic) aortic arch leads to enhanced systolic wave reflection, central aortic stiffness, and increased left ventricular mass late after aortic coarctation repair: evaluation with magnetic resonance flow mapping, J. Thorac. Cardiovasc. Surg. 135 (2008) 62–68, https://doi.org/10.1016/j.jtcvs.2007.03.059.
[45] A. Frydrychowicz, A. Berger, A. Munoz Del Rio, M.F. Russe, J. Bock, A. Harloff, M. Markl, Interdependencies of aortic arch secondary flow patterns, geometry, and age analysed by 4-dimensional phase contrast magnetic resonance imaging at 3 Tesla, Eur. Radiol. 22 (2012) 1122–1130, https://doi.org/10.1007/s00330-011-2353-6.
[46] M.E. Casciaro, D. Craiem, G. Chironi, S. Graf, L. Macron, E. Mousseaux, A. Simon, R.L. Armentano, Identifying the principal modes of variation in human thoracic aorta morphology, J. Thorac. Imaging 29 (2014) 224–232, https://doi.org/10.1097/RTI.0000000000000060.
[47] F. Cosentino, G.M. Raffa, G. Gentile, V. Agnese, D. Bellavia, M. Pilato, S. Pasta, Statistical shape analysis of ascending thoracic aortic aneurysm: correlation between shape and biomechanical descriptors, J. Pers. Med. 10 (2020) 28, https://doi.org/10.3390/jpm10020028.
[48] E.M. Isselbacher, O. Preventza, J. Hamilton Black, J.G. Augoustides, A.W. Beck, M. A. Bolen, A.C. Braverman, B.E. Bray, M.M. Brown-Zimmerman, E.P. Chen, et al., 2022 ACC/AHA guideline for the diagnosis and management of aortic disease: a report of the American Heart Association/American College of Cardiology Joint Committee on Clinical Practice Guidelines, Circulation 146 (2022), https://doi.org/10.1161/CIR.0000000000001106.
[49] D. Gallo, D.A. Steinman, U. Morbiducci, An insight into the mechanistic role of the common carotid artery on the hemodynamics at the carotid bifurcation, Ann. Biomed. Eng. 43 (2015) 68–81, https://doi.org/10.1007/s10439-014-1119-0).
[50] A. Guala, A. Evangelista, G. Teixido-Tura, L. La Mura, L. Dux-Santoy, A. Ruiz-Muñoz, F. Valente, L. Galian-Gay, L. Gutiérrez, T. González-Alujas, et al., Leaflet fusion length is associated with aortic dilation and flow alterations in non-dysfunctional bicuspid aortic valve, Eur. Radiol. 31 (2021) 9262–9272, https://doi.org/10.1007/s00330-021-08016-3.
[51] A. Guala, J. Rodriguez-Palomares, L. Dux-Santoy, G. Teixido-Tura, G. Maldonado, L. Galian, M. Huguet, F. Valente, L. Gutiérrez, T. González-Alujas, et al., Influence of aortic dilation on the regional aortic stiffness of bicuspid aortic valve assessed by 4-dimensional flow cardiac magnetic resonance: comparison with marfan syndrome and degenerative aortic aneurysm, JACC Cardiovasc. Imaging 12 (2019) 1020–1029, https://doi.org/10.1016/j.jcmg.2018.03.017.
[52] L. Shahid, J. Rice, H. Berhane, C. Rigsby, J. Robinson, L. Griffin, M. Markl, A. Roldán-Alzate, Enhanced 4D flow MRI-based CFD with adaptive mesh refinement for flow dynamics assessment in coarctation of the aorta, Ann. Biomed. Eng. 50 (2022) 1001–1016, https://doi.org/10.1007/s10439-022-02980-7.
[53] J.G. Williams, D. Marlevi, J.L. Bruse, F.R. Nezami, H. Moradi, R.N. Fortunato, S. Maiti, M. Billaud, E.R. Edelman, T.G. Gleason, Aortic dissection is determined by specific shape and hemodynamic interactions, Ann. Biomed. Eng. 50 (2022) 1771–1786, https://doi.org/10.1007/s10439-022-02979-0).
[54] M.D. Hope, T.A. Hope, A.K. Meadows, K.G. Ordovas, T.H. Urbania, M.T. Alley, C. B. Higgins, Bicuspid aortic valve: four-dimensional MR evaluation of ascending aortic systolic flow patterns, Radiology 255 (2010) 53–61, https://doi.org/10.1148/radiol.09091437.
[55] L. Dux-Santoy, A. Guala, G. Teixidó-Turà, A. Ruiz-Muñoz, G. Maldonado, N. Villalva, L. Galian, F. Valente, L. Gutiérrez, T. González-Alujas, et al., Increased rotational flow in the proximal aortic arch is associated with its dilation in bicuspid aortic valve disease, Eur. Heart J. Cardiovasc. Imaging 20 (2019) 1407–1417, https://doi.org/10.1093/ehjci/jez046.
[56] S. Pirola, O.A. Jarral, D.P. O'Regan, G. Asimakopoulos, J.R. Anderson, J.R. Pepper, T. Athanasiou, X.Y. Xu, Computational study of aortic hemodynamics for patients with an abnormal aortic valve: the importance of secondary flow at the ascending aorta inlet, APL Bioeng. 2 (2018) 26101, https://doi.org/10.1063/1.5011960.
[57] E.K. Weiss, K. Jarvis, A. Maroun, S.C. Malaisrie, C.K. Mehta, P.M. McCarthy, R. O. Bonow, R.J. Avery, B.D. Allen, J.C. Carr, et al., Systolic reverse flow derived from 4D flow cardiovascular magnetic resonance in bicuspid aortic valve is associated with aortic dilation and aortic valve stenosis: a cross sectional study in 655 subjects, J. Cardiovasc. Magn. Reson. 25 (2023) 3, https://doi.org/10.1186/s12968-022-00906-9.
[58] D.Z. Gordon, M.A. Abbasi, J. Lee, R. Sarnari, A. Sojoudi, Q. Wei, M.B. Scott, J. D. Collins, B.D. Allen, J.A. Blaisdell, et al., Four-dimensional flow magnetic resonance imaging quantification of blood flow in bicuspid aortic valve, J. Thorac. Imaging 35 (2020) 383–388, https://doi.org/10.1097/RTI.0000000000000535.
[59] P. Geeraert, F. Jamalidinan, F. Burns, K. Jarvis, M.S. Bristow, C. Lydell, S. S. Hidalgo Tobon, B. de Celis Alonso, P.W.M. Fedak, J.A. White, et al., Hemodynamic assessment in bicuspid aortic valve disease and aortic dilation: new insights from voxel-by-voxel analysis of reverse flow, stasis, and energetics, Front. Bioeng. Biotechnol. 9 (2022), https://doi.org/10.3389/fbioe.2021.725113.
[60] J.D. Collins, E. Semaan, A.M. Barker, P. McCarthy, J.C. Carr, M. Markl, S. C. Malaisrie, Comparison of hemodynamics after aortic root replacement using valve-sparing or bioprosthetic valved conduit, Ann. Thorac. Surg. 100 (2015) 1556–1562, https://doi.org/10.1016/j.athoracsur.2015.04.109.
[61] E. Semaan, M. Markl, S. Chris Malaisrie, A. Barker, B. Allen, P. McCarthy, J.C. Carr, J.D. Collins, Haemodynamic outcome at four-dimensional flow magnetic resonance imaging following valve-sparing aortic root replacement with tricuspid and bicuspid valve morphology, Eur. J. Cardio Thorac. Surg. 45 (2014) 818–825, https://doi.org/10.1093/ejcts/ezt526.
[62] F.M. Callaghan, P. Bannon, E. Barin, D. Celemajer, R. Jeremy, G. Figtree, S. M. Grieve, Age-related changes of shape and flow dynamics in healthy adult aortas: a 4D flow MRI study, J. Magn. Reson. Imaging 49 (2019) 90–100, https://doi.org/10.1002/jmri.26210.

[63] M.B. Scott, H. Huh, P. van Ooij, V. Chen, B. Herrera, M. Elbaz, P. McCarthy, S. C. Malaisrie, J. Carr, P.W.M. Fedak, et al., Impact of age, sex, and global function on normal aortic hemodynamics, Magn. Reson. Med. 84 (2020) 2088–2102, https://doi.org/10.1002/mrm.28250.

[64] E.T. Bieging, A. Frydrychowicz, A. Wentland, B.R. Landgraf, K.M. Johnson, O. Wieben, C.J. François, *In vivo* three-dimensional MR wall shear stress estimation in ascending aortic dilatation, J. Magn. Reson. Imaging 33 (2011) 589–597, https://doi.org/10.1002/jmri.22485.

[65] K.M. Tse, R. Chang, H.P. Lee, S.P. Lim, S.K. Venkatesh, P. Ho, A computational fluid dynamics study on geometrical influence of the aorta on haemodynamics, Eur. J. Cardio Thorac. Surg. 43 (2013) 829–838, https://doi.org/10.1093/ejcts/ezs388.

[66] M.D. Hope, J. Wrenn, M. Sigovan, E. Foster, E.E. Tseng, D. Saloner, Imaging biomarkers of aortic disease, J. Am. Coll. Cardiol. 60 (2012) 356–357, https://doi.org/10.1016/j.jacc.2012.01.072.

[67] M.M. Bissell, A.T. Hess, L. Biasiolli, S.J. Glaze, M. Loudon, A. Pitcher, A. Davis, B. Prendergast, M. Markl, A.J. Barker, et al., Aortic dilation in bicuspid aortic valve disease, Circ. Cardiovasc. Imaging 6 (2013) 499–507, https://doi.org/10.1161/CIRCIMAGING.113.000528.

[68] M.D. Hope, T.A. Hope, S.E.S. Crook, K.G. Ordovas, T.H. Urbania, M.T. Alley, C. B. Higgins, 4D Flow CMR in assessment of valve-related ascending aortic disease, JACC Cardiovasc. Imaging 4 (2011) 781–787, https://doi.org/10.1016/j.jcmg.2011.05.004.

[69] L. Dux-Santoy, A. Guala, J. Sotelo, S. Uribe, G. Teixidó-Turà, A. Ruiz-Muñoz, D. E. Hurtado, F. Valente, L. Galian-Gay, L. Gutiérrez, et al., Low and oscillatory wall shear stress is not related to aortic dilation in patients with bicuspid aortic valve, Arterioscler. Thromb. Vasc. Biol. 40 (2020), https://doi.org/10.1161/ATVBAHA.119.313636.

[70] A.J. Barker, M. Markl, J. Bürk, R. Lorenz, J. Bock, S. Bauer, J. Schulz-Menger, F. von Knobelsdorff-Brenkenhoff, Bicuspid aortic valve is associated with altered wall shear stress in the ascending aorta, Circ. Cardiovasc. Imaging 5 (2012) 457–466, https://doi.org/10.1161/CIRCIMAGING.112.973370.

[71] D.G. Guzzardi, A.J. Barker, P. van Ooij, S.C. Malaisrie, J.J. Puthumana, D.D. Belke, H.E.M. Mewhort, D.A. Svystonyuk, S. Kang, S. Verma, et al., Valve-related hemodynamics mediate human bicuspid aortopathy: insights from wall shear stress mapping, J. Am. Coll. Cardiol. 66 (2015) 892–900, https://doi.org/10.1016/j.jacc.2015.06.1310.